Stable Highly Doped $C_{60-m}Si_m$ Heterofullerenes: A First Principles Study of $C_{40}Si_{20}$, $C_{36}Si_{24}$, and $C_{30}Si_{30}$

Masahiko Matsubara and Carlo Massobrio*

Institut de Physique et Chimie des Matériaux de Strasbourg, 23 rue du Loess, BP 43 F-67034 Strasbourg Cedex 2, France

Received: March 16, 2005

Geometry optimization within the framework of density functional theory provides clear evidence of stable fullerene-like cage structures for $C_{40}Si_{20}$, $C_{36}Si_{24}$, and $C_{30}Si_{30}$. In the case of $C_{40}Si_{20}$, an extensive isomer search shows that the most stable arrangements are those in which the Si atoms and the C atoms form two distinct homogeneous subnetworks. Any other configuration corresponding to spatially separated sets of Si atoms leads to a decrease of the binding energy. Due to charge transfer from Si to C atoms, opposite charges are found in neighboring Si and C sites. Structural stability is ensured via the predominant occurrence of 3-fold bonding for both species.

Substitutional Si-doping of fullerenes aims at the synthesis of new nanosystems combining enhanced chemical reactivity with reduced structural modifications of the original cage structures.[1−5] A tentative upper limit of 12 C atoms replaced by Si atoms has been established via mass spectrometry and photofragmentation studies on $C_{2n-m}Si_m$ clusters, with $2n = 32-80$.[4,5] On the theoretical side, various approaches showed that the Si_{60} hollow, fullerene-like configuration relaxes into a drastically different arrangement ("puckered ball").[6−8] At the opposite range of compositions, structural and electronic properties of Si-doped $C_{60-m}Si_m$ heterofullerenes for $m \leq 12$ have been characterized very recently.[9−15] In these systems, the C_{60} cage structure is distorted and yet preserved, structural deformation taking place in the vicinity of the dopant atoms, with Si−C and Si−Si bonds larger than C−C bonds. For $m \geq 3$, the most stable structures are those where the Si atoms form a distinct subunit, resulting in a segregated pattern that confines C and Si atoms in separate regions.[12−15]

To date, it remains to be determined whether C_{60-m} clusters can host a number of Si atoms larger than $m = 12$, while retaining a cage-like structural character still bearing some resemblance with C_{60}. To address this issue, we focus in this paper on the structural stability at $T = 0$ K of $C_{40}Si_{20}$, $C_{36}Si_{24}$ and $C_{30}Si_{30}$ via density functional theory (DFT) calculations combined with geometry optimization. We found that the lowest energy configurations consist of two clearly distinct subnetworks forming a distorted closed cage. On one hand, C atoms do preserve the conjugated pattern of distances typical of C_{60} in a regular arrangement. On the other hand, Si−Si bonds are larger and concur to create a protruding network capping the cluster. An extended isomer search performed for $C_{40}Si_{20}$ confirms that nanoscale segregation is the key factor stabilizing Si-doped heterofullerenes. This concept is used to construct stable structures for $C_{36}Si_{24}$ and $C_{30}Si_{30}$.

In our calculations, we employ DFT with generalized gradient approximations (GGA) after Becke (B)[16] for the exchange energy and Lee, Yang, and Parr (LYP)[17] for the correlation energy.[18] The core-valence interaction is described by norm-conserving pseudopotentials of the Troullier−Martins type.[19] Structural optimization is performed within the framework of the Car−Parrinello molecular dynamics.[20,21] The use of periodic boundary conditions requires a computational cell large enough to minimize the interactions among periodically repeated images. These conditions are met by adopting a face-centered cubic cell with an edge of 21.17 Å. Wave functions are expanded in plane waves with an energy cutoff of 40 Ry. For $C_{40}Si_{20}$, initial configurations are obtained as follows. We took the optimized structures of $C_{48}Si_{12}$ by imposing new C−Si replacements in the neighborhood of Si atoms.[15] Alternatively, we distributed Si atoms in spatially distinct groups. This corresponds to the inclusion of C atoms in paths connecting given pairs of Si atoms. Initial structures of $C_{36}Si_{24}$ and $C_{30}Si_{30}$ are constructed from the most stable isomers of $C_{40}Si_{20}$ by considering only homogeneous Si regions. In all cases, optimization of the ionic positions is performed without constraint on the structure and is allowed to proceed until the largest force component is less than 0.026 eV/Å.

A schematic view of the optimized configurations for 11 isomers of $C_{40}Si_{20}$ is given in Figure 1, where we employed a two-dimensional representation as a guide to the eye. The most stable structures result from the combined tendency of Si atoms to stick together and form weak sp^2 bonding. Among the eight lowest isomers lying within 1.40 eV (∼0.02 eV/atom), six have in common the same number of Si−Si bonds ($N_{Si-Si} = 25$), of Si−C bonds ($N_{Si-C} = 10$), and of Si atoms 3-fold coordinated with Si atoms ($N_{Si3-fold} = 10$) (isomers **A**−**D**, **F**, **G**). They all consist of six completed polygons. In the most stable, a central pentagon is surrounded by five hexagons, with the largest number, 10, of Si−Si hh (hexagon−hexagon) bonds. In isomers **E** and **H**, of binding energy comparable to the above six, the values are $N_{Si-Si} = 24$, $N_{Si-C} = 12$, and $N_{Si3-fold} = 8$. This shows that a simple trend of stability cannot be extracted from a count of bonds and coordination for configurations exhibiting a single Si-made region.

As shown in Table 1, Si−Si distances do not exceed 2.52 Å, with most values ranging between 2.30 and 2.45 Å. It appears that increased doping does not stretch significantly the Si−Si bonds, confirming the trend observed in ref 14. Also, the conjugated pattern of C−C bonds persists for increased Si content, with the pentagon−hexagon (ph) bonds larger than the hh ones. The ph and hh bonds follow this same pattern for Si−C bonds (see Table 1 for the isomers containing both of them).

10.1021/jp058094s CCC: $30.25
Published on Web 04/22/2005

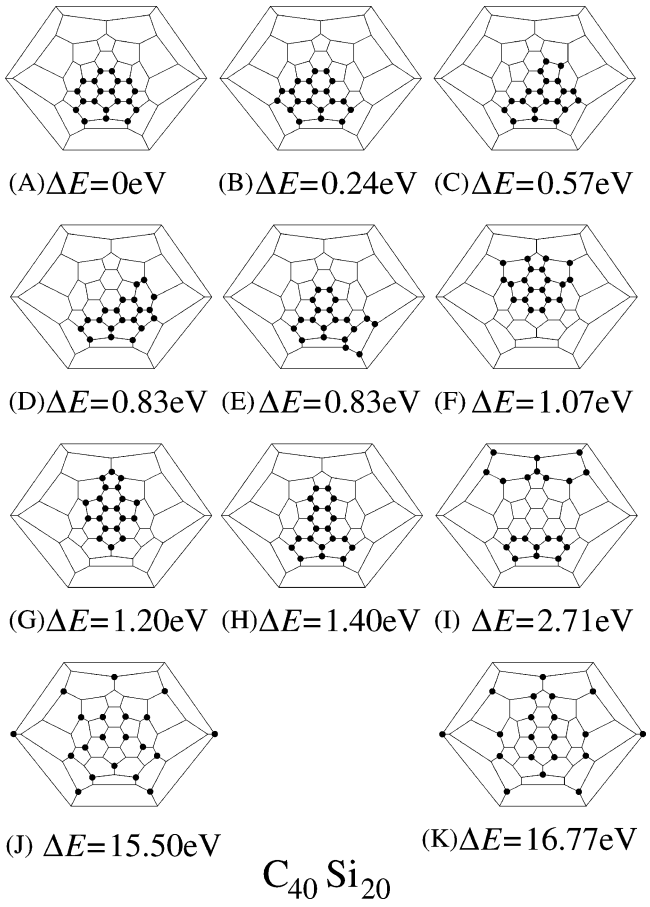

Figure 1. Schematic representation of Si atom locations (black dots) in $C_{40}Si_{20}$ isomers. The flattened view is a guide to the eye. Bond distances are not intended to reflect real interatomic distances.

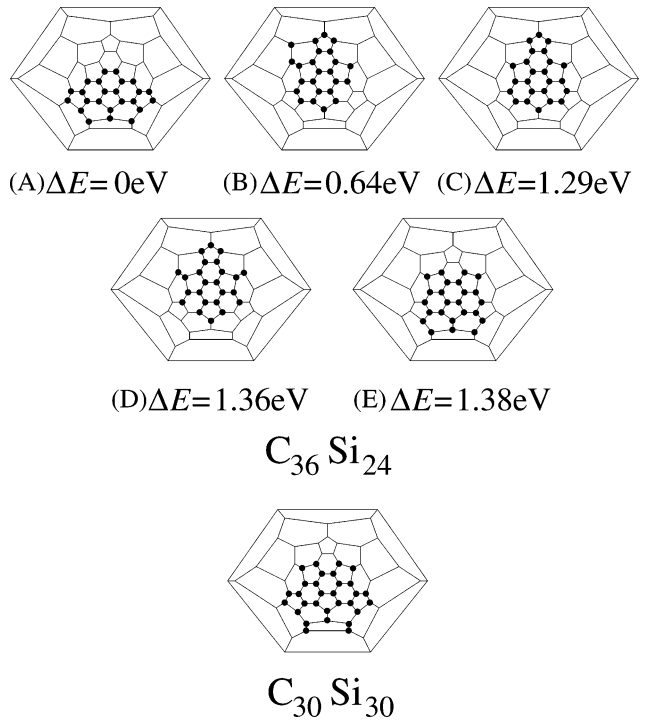

Figure 2. Schematic representation of Si atom locations (black dots) in $C_{36}Si_{24}$ and $C_{30}Si_{30}$ isomers. The flattened view is a guide to the eye. Bond distances are not intended to reflect real interatomic distances.

Separating Si atoms in two or more regions (isomers **I**−**K** in Figure 1) decreases notably the binding energy, due to the high energetic cost (as much as ∼0.25 eV/atom) associated with the creation of Si−C bonds at the expenses of Si−Si bonds.

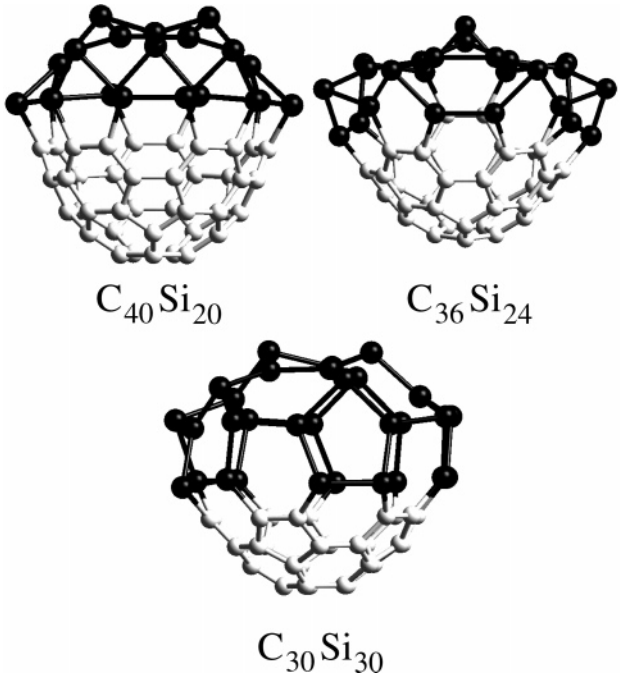

Figure 3. Ball and stick representation of the structures of the most stable isomers of $C_{40}Si_{20}$, $C_{36}Si_{24}$, and $C_{30}Si_{30}$ (one structure considered in this latter case). The black and gray atoms are silicon and carbon atoms, respectively.

Moving to a higher content of Si dopant atoms, we optimized five structures for $C_{36}Si_{24}$. This is done by imposing four additional C−Si replacements in isomers **A** and **B** (two and three cases considered, respectively) of $C_{40}Si_{20}$ (Figure 2). All structures contain eight polygons. The most stable is obtained from isomer **A** of $C_{40}Si_{20}$ and it has two more Si_5 pentagons. Overall, interatomic distances reflect the remarkable tendency of the two sets of atoms to organize themselves so as to maintain the alternate single-bond/double bond pattern (C atoms) and arrange in a sp^2-like fashion (Si atoms). As shown in Table 2, Si−Si distances as long as 2.58 Å can be found in two isomers of $C_{36}Si_{24}$. Such bond lengths are not necessarily precursor of cluster fragmentation, as indicated in a previous molecular dynamics study by the behavior with temperature of $C_{54}Si_6$.[14] In that case, two Si atoms were separated at $T = 0$ K by 2.66 Å and yet the cluster did not fall apart on a time interval of 12 ps at $T = 3000$ K.

The above considerations prompted us to optimize the structure given in Figure 2 for $C_{30}Si_{30}$. This heterofullerene is made of 5 hexagons and 5 pentagons. Bond lengths are fully consistent with the stability of this highly doped fullerene. We note that Si−Si bonds are between 2.30 and 2.48 Å, Si−C bonds range from 1.85 and 1.91 Å and C−C bonds are organized in two distinct sets of ph and hh bonds (Table 2). Therefore, our calculations provide support to the notion of a fully half-doped substitutional fullerene retaining a cage-like structure. Consideration of singly charged (positive or negative) isomers does not affect this conclusion, as it will be shown in detail elsewhere.[22] Increased doping goes along with a decrease in binding energy E_b of as much as 2 eV with respect to C_{60} [$E_b(C_{60}) = 8.17$ eV/atom, $E_b(C_{40}Si_{20}) = 6.81$ eV/atom, $E_b(C_{30}Si_{30}) = 6.13$ eV/atom]. However, the relative energy change is larger when moving from C_{60} to $C_{40}Si_{20}$ (16%) than when moving from $C_{40}Si_{20}$ to $C_{30}Si_{30}$ (9%).

TABLE 1: Calculated Bond Lengths of $C_{40}Si_{20}$[a]

isomers		Si−Si (Å)		Si−C (Å)		C−C (Å)
A	ph	2.37 × 2, 2.38 × 2, 2.39 × 2, 2.40 2.41 × 5, 2.44, 2.47 × 2	ph	1.89 × 2, 1.90 × 2, 1.91 × 2 1.97 × 2, 1.98 × 2	ph	1.46−1.52
	hh	2.31 × 3, 2.32 × 2, 2.36 × 2 2.42, 2.46, 2.47			hh	1.41−1.43
B	ph	2.33 × 2, 2.34, 2.37, 2.39, 2.40 × 5 2.41 × 2, 2.43, 2.46, 2.47 × 2	ph	1.89, 1.91, 1.92 × 2 1.93 × 2, 1.94, 2.05	ph	1.45−1.51
	hh	2.32, 2.34, 2.35 × 2, 2.41 2.42, 2.45 × 2, 2.48	hh	1.84 × 2	hh	1.41−1.45
C	ph	2.33, 2.35, 2.36 × 2, 2.37 × 2, 2.38, 2.39 × 2 2.40 × 3, 2.41 × 3, 2.42, 2.43, 2.48	ph	1.91 × 2, 1.92, 1.95	ph	1.45−1.51
	hh	2.31, 2.34, 2.35, 2.36 × 2, 2.40, 2.42	hh	1.83 × 2, 1.86, 1.87, 1.91, 1.94	hh	1.40−1.45
D	ph	2.33, 2.35 × 3, 2.38 × 3, 2.39 × 2 2.42 × 3, 2.44, 2.46, 2.50, 2.51	ph	1.89, 1.91, 1.92 × 3 1.95, 1.99, 2.00	ph	1.45−1.52
	hh	2.34, 2.35 × 4, 2.37, 2.38, 2.40, 2.45	hh	1.84, 1.85	hh	1.41−1.45
E	ph	2.35 × 3, 2.36, 2.37 × 2, 2.38 × 3 2.39 × 2, 2.40 × 2, 2.46	ph	1.89 × 2, 1.91 × 2, 1.94 × 3 1.96 × 3, 1.97, 2.03	ph	1.45−1.53
	hh	2.30, 2.32, 2.33 × 2, 2.35 2.36 × 2, 2.39, 2.41 × 2			hh	1.40−1.43
F	ph	2.32 × 2, 2.33 × 2, 2.34, 2.37, 2.38 × 2 2.39, 2.40 × 3, 2.42 × 2, 2.43 × 2	ph	1.88, 1.90, 1.91 × 2 1.96 × 2, 1.97, 1.99	ph	1.45−1.53
	hh	2.32 × 2, 2.34 × 2, 2.35 × 2 2.38, 2.39, 2.40	hh	1.84, 1.85	hh	1.40−1.44
G	ph	2.30, 2.32 × 2, 2.35, 2.36 2.37 × 3, 2.39 × 6, 2.41 × 4, 2.42 × 2			ph	1.45−1.49
	hh	2.36 × 4, 2.39	hh	1.84 × 2, 1.86 × 4, 1.88 × 2, 1.91 × 2	hh	1.40−1.44
H	ph	2.33, 2.34, 2.36 × 3, 2.37 × 3 2.39 × 3, 2.42, 2.43, 2.47	ph	1.88 × 2, 1.90, 1.91, 1.92, 1.94 1.97, 1.99 × 2, 2.01 × 2, 2.03	ph	1.45−1.52
	hh	2.28, 2.32, 2.33, 2.35, 2.36 2.38 × 2, 2.40 × 2, 2.41			hh	1.40−1.43
I	ph	2.36, 2.37 × 3, 2.38, 2.39, 2.40 × 2 2.41, 2.42, 2.43, 2.52	ph	1.88, 1.89, 1.90 × 2, 1.91 × 3, 1.92 1.94, 1.96 × 3, 1.97, 1.99, 2.00, 2.01	ph	1.45−1.51
	hh	2.31 × 2, 2.33, 2.34 × 2, 2.35 2.38, 2.40, 2.43, 2.46			hh	1.41−1.43
J			ph	1.84 × 2, 1.85 × 2, 1.86 × 2, 1.87 × 6 1.88 × 8, 1.89 × 6, 1.90 × 2, 1.91 × 4 1.92 × 2, 1.93 × 2, 1.98 × 2, 1.99, 2.00	ph	1.42−1.51
			hh	1.79, 1.81 × 2, 1.83 × 2, 1.85 × 2 1.86 × 7, 1.87 × 2, 1.89 × 2, 1.90 × 2	hh	1.39−1.45
K			ph	1.83 × 2, 1.86 × 6, 1.87 × 2, 1.88 × 5 1.89 × 9, 1.90 × 7, 1.91, 1.93 × 2 1.94 × 2, 1.95 × 2, 1.96 × 2	ph	1.42−1.54
			hh	1.82 × 4, 1.84 × 4, 1.87 × 4 1.88 × 4, 1.89 × 4	hh	1.39−1.45

[a] For the C−C bond lengths, the smallest and the largest values found are shown. The distances are expressed in Å.

TABLE 2: Calculated Bond Lengths of $C_{36}Si_{24}$ and $C_{30}Si_{30}$[a]

isomers		Si−Si (Å)		Si−C (Å)		C−C (Å)
			$C_{36}Si_{24}$			
A	ph	2.33 × 2, 2.34 × 2, 2.37 × 2, 2.40 × 2 2.41 × 6, 2.42, 2.47 × 4, 2.48 × 2	ph	1.91 × 2, 1.92 × 3, 1.93	ph	1.45−1.52
	hh	2.33 × 3, 2.43 × 4, 2.46, 2.48 × 2	hh	1.84 × 2, 1.85 × 2	hh	1.40−1.44
B	ph	2.32, 2.34, 2.35 × 2, 2.36, 2.37 × 2 2.38 × 2, 2.39, 2.40 × 4, 2.41, 2.46 2.47, 2.48 × 2, 2.51 × 2, 2.58	ph	1.90 × 2, 1.94 × 2	ph	1.45−1.49
	hh	2.34, 2.35 × 3, 2.36, 2.38 × 2, 2.40 × 2	hh	1.84 × 2, 1.85 × 2, 1.92 × 2	hh	1.40−1.45
C	ph	2.33 × 2, 2.34 × 2, 2.35 × 4, 2.37 × 4 2.39 × 2, 2.40 × 4, 2.43, 2.44 × 2, 2.57	ph	1.89 × 2, 1.99 × 2	ph	1.45−1.50
	hh	2.29, 2.34 × 2, 2.36 × 2, 2.37 × 4	hh	1.84, 1.88 × 3, 1.91 × 2	hh	1.40−1.44
D	ph	2.30, 2.32, 2.34 × 2, 2.35, 2.36, 2.37 2.38 × 2,2.39 × 3, 2.40, 2.42 × 3 2.43, 2.44, 2.50, 2.52	ph	1.86 × 3, 1.89, 1.91 × 2 1.92, 1.95	ph	1.46−1.51
	hh	2.28, 2.32, 2.33 × 2 2.35 × 2, 2.38, 2.41 × 2	hh	1.83, 1.84, 1.85 × 2 1.90, 1.91	hh	1.40−1.46
E	ph	2.31, 2.32 × 2, 2.33, 2.35 × 2, 2.36 2.37, 2.38, 2.39 × 3, 2.40 × 3, 2.41 2.43, 2.44 × 2, 2.46, 2.58	ph	1.90 × 2, 1.91 × 2, 1.96 1.97	ph	1.45−1.51
	hh	2.31 × 4, 2.35, 2.40 2.43 × 2, 2.44, 2.46	hh	1.86 × 2, 1.88,1.89	hh	1.40−1.45
			$C_{30}Si_{30}$			
	ph	2.30 × 2, 2.33 × 2, 2.34 × 4, 2.35 × 2 2.36 × 2, 2.38 × 2, 2.39 × 3, 2.40 × 9 2.41 × 2, 2.42, 2.48			ph	1.45−1.49
	hh	2.31, 2.34 × 2, 2.35 2.36 × 2, 2.38 × 3, 2.40	hh	1.85 × 4, 1.86, 1.87 × 2 1.88, 1.89, 1.91	hh	1.40−1.44

[a] For the C−C bond lengths, the smallest and the largest values found are shown. The distances are expressed in Å.

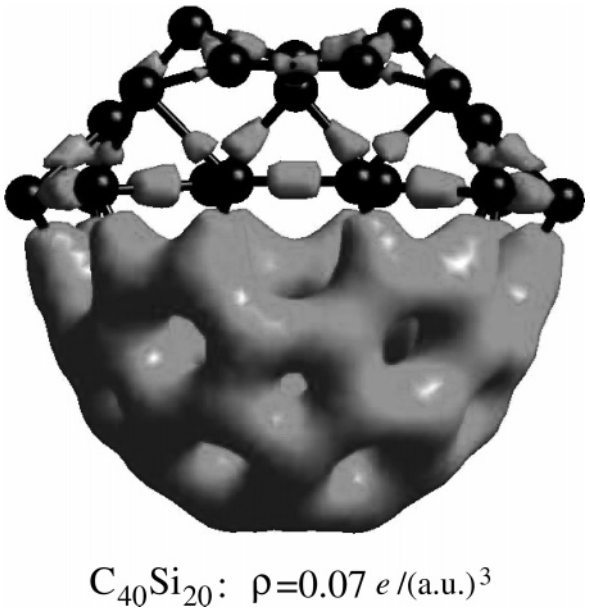

Figure 4. Probability isodensity surface associated with the total valence charge density at $\rho = 0.07$ e/(a.u.)^3 for the most stable isomer of $C_{40}Si_{20}$.

More insight into the structures is given by the three-dimensional views of Figure 3 for the most stable isomers of $C_{40}Si_{20}$, $C_{36}Si_{24}$, and the single case of $C_{30}Si_{30}$. These heterofullerenes have in common the marked configurational transition occurring from one subnetwork to the other, consistent with the different propensity of C and Si atoms to accommodate three nearest neighbors. On going from the C to the Si-populated region, the cage widens to allow for Si atoms to find a location within it. By focusing on the distances between pairs of atoms as a measure of the cluster size, the largest value for C atoms is found in $C_{40}Si_{20}$ (8.11 Å), to be compared with 7.20 Å in C_{60}. Larger distances are found for Si atoms, up to 11.07 Å in $C_{36}Si_{24}$. We recall that Si−C bonding in $C_{59}Si$ was rationalized by ruling out sp^3 bonding via a Wannier function analysis.[9] In the present case, Si atoms are able to cap the fullerene via Si−Si−Si triads involving angles largely scattered (by ∼20°) around an average value close to 109.5°, the perfect tetrahedral angle. This points out that further doping is expected to favor even more sp^3 bonding, at the expenses of weak or distorted sp^2 bonding, in agreement with the conclusions of ref 7 for Si_{60}.

Changes in electronic properties caused by doping of fullerenes have the effect of creating new reactive sites.[9,14] Bonding in Si-doped heterofullerenes is characterized by charge transfer from the Si atoms to the more electronegative C atoms. As a general trend, it can be shown that, for a given Si (C) atom, the amount of positive (negative) charge increases with an increasing number of C (Si) nearest neighbors.[14] In the case of C atoms, we found significant negative charges (up to 0.2) for those C atoms bonding Si atoms. In turn, neighboring Si atoms have the largest positive values (0.2−0.3). Leaving the border of the Si−C interface to move inward, Si-made regions, Si atoms take vanishingly positive or small negative values (up to −0.1) when surrounded by three neighbors of the same kind. Therefore, the observed structural segregation results in an overall electronic charge transfer from the Si-populated to the C-populated regions. We confirm this description via the plot of the electron density ρ shown in Figure 4, for the isosurface corresponding to $\rho = 0.07$ e/(au)^3. One notes the highly nonhomogeneous character of the electronic density that spreads over the C atoms along the bonding directions. Due to charge transfer, much less is noticeable in the region where the Si atoms reside. Indeed, the electron density appears in pockets of limited extension located in the middle of the Si−Si bonds.

The stability of highly Si-doped fullerenes should stimulate experimental efforts to establish whether the above findings have a realistic experimental counterpart. Our results indicate that plausible configurations can be obtained provided the two species involved do not share the same regions in the cage. For the dopant atom, this gives rise to preferential clustering of predominantly positive charges and neighboring negatively charged C atoms. It appears that enhanced polarization is a novel feature peculiar to $C_{60-m}Si_m$ systems with high m, altering the purely covalent bonding character of undoped fullerenes.

To improve upon the present results, one needs to focus on the role played by the temperature. This goal can be achieved by first disentangling the mechanisms of thermal motion well before fragmentation and then directly looking for the fragmentation processes.[14,23−25] We are currently addressing this issue via first-principles molecular dynamics simulation at finite temperatures.

Acknowledgment. Calculations have been carried out on the computers of the French national centers IDRIS (Orsay) and CINES (Montpellier).

References and Notes

(1) Kimura, T.; Sugai, T.; Shinohara, H. *Chem. Phys. Lett.* **1996**, *256*, 269.
(2) Fye, J. L.; Jarrold, M. F. *J. Phys. Chem. A* **1997**, *101*, 1836.
(3) Ray, C.; Pellarin, M.; Lermé, J. L.; Vialle, J. L.; Broyer, M.; Blase, X.; Mélinon, P.; Kéghélian, P.; Perez, A. *Phys. Rev. Lett.* **1998**, *80*, 5365.
(4) Pellarin, M.; Ray, C.; Lermé, J.; Vialle, J. L.; Broyer, M.; Blase, X.; Kéghélian, P.; Mélinon, P.; Perez, A. *J. Chem. Phys.* **1999**, *110*, 6927.
(5) Pellarin, M.; Ray, C.; Lermé, J.; Vialle, J. L.; Broyer, M.; Blase, X.; Kéghélian, P.; Mélinon, P.; Perez, A. *Eur. Phys. J. D* **1999**, *9*, 49.
(6) Kahn, F. S.; Broughton, J. Q. *Phys. Rev. B* **1991**, *43*, 11754.
(7) Menon, M.; Subbaswamy, K. R. *Chem. Phys. Lett.* **1994**, *219*, 219.
(8) Li, B.-X.; Jiang, M.; Cao, P.-L. *J. Phys. Condens. Matter* **1999**, *11*, 8517.
(9) Billas, I. M. L.; Massobrio, C.; Boero, M.; Parrinello, M.; Branz, W.; Tast, F.; Malinowski, N.; Heinebrodt, M.; Martin, T. P. *J. Chem. Phys.* **1999**, *111*, 6787.
(10) Billas, I. M. L.; Tast, F.; Branz, W.; Malinowski, N.; Heinebrodt, M.; Martin, T. P.; Boero, M.; Massobrio, C. *Eur. Phys. J. D* **1999**, *9*, 337.
(11) Billas, I. M. L.; Branz, W.; Malinowski, N.; Tast, F.; Heinebrodt, M.; Martin, T. P.; Massobrio, C.; Boero, M.; Parrinello, M. *Nanostruct. Mater.* **1999**, *12*, 1071.
(12) Fu, C.-C.; Weissmann, M.; Machado, M.; Ordejón, P. *Phys. Rev. B* **2001**, *63*, 085411.
(13) Menon, M. *J. Chem. Phys.* **2001**, *114*, 7731.
(14) Matsubara, M.; Massobrio, C. *J. Chem. Phys.* **2005**, *122*, 084304.
(15) Matsubara, M.; Massobrio, C.; Parlebas, J. C. *Comput. Mater. Sci.* **2005**, *33*, 237.
(16) Becke, A. D. *Phys. Rev. A* **1988**, *38*, 3098.
(17) Lee, C.; Yang, W.; Parr, R. G. *Phys. Rev. B* **1988**, *37*, 785.
(18) The BLYP approximation for the gradient corrections of the exchange and correlation energy gives reliable results in the case of carbon systems, whereas other GGAs are not equally well assessed for large carbon molecules, [see, e.g.: Johnson, B. G.; Gill, P. M. W.; Pople, J. A. *J. Chem. Phys.* **1993**, *98*, 5612. Curtiss, L. A.; Raghavashari, K.; Redfern, P. C.; Pople, J. A. *J. Chem. Phys.* **1997**, *106*, 1063. Ernzerhof, M.; Scuseria, G. E. *J. Chem. Phys.* **1999**, *110*, 5029].
(19) Troullier, N.; Martins, J. L. *Phys. Rev. B* **1991**, *43*, 1993.
(20) Car, R.; Parrinello, M. *Phys. Rev. Lett.* **1985**, *55*, 2471.
(21) We have used the code CPMD: CPMD Version 3.7.1 and 3.7.2, Copyright IBM Corp (1990−2003) and MPI für Festkörperforschung Stuttgart (1997−2001).
(22) Matsubara, M.; Massobrio, C. Unpublished results.
(23) Fu, C.-C.; Fava, J.; Weht, R.; Weissmann, M. *Phys. Rev. B* **2002**, *66*, 045405.
(24) Marcos, P. A.; Alonso, J. A.; Molina, L. M.; Rubio, A.; López, M. J. *J. Chem. Phys.* **2003**, *119*, 1127.
(25) Ramaniah, L. M.; Boero, M.; Laghate, M. *Phys. Rev. B* **2004**, *70*, 035411.